Stability Tools for the Spectral-Element Code Nek5000; Application to Jet-in-Crossflow

A. Peplinski, P. Schlatter, P. F. Fischer, and D. S. Henningson

Abstract We demonstrate the use of advanced linear stability tools developed for the spectral-element code `Nek5000` to investigate the dynamics of nonlinear flows in moderately complex geometries. The aim of stability calculations is to identify the driving mechanism as well as the region most sensitive to the instability: the *wavemaker*. We concentrate on global linear stability analysis, which considers the linearised Navier–Stokes equations and searches for growing small disturbances, *i.e.* so-called linear global modes. In the structural sensitivity analysis these modes are associated to the eigenmodes of the direct and adjoint linearised Navier–Stokes operators, and the wavemaker is defined as the overlap of the strongest direct and adjoint eigenmodes. The large eigenvalue problems are solved using matrix–free methods adopting the time–stepping Arnoldi approach. We present here our implementation in `Nek5000` with the `ARPACK` library on a number of test cases.

1 Introduction

The flow of fluids can be either laminar, characterised by smooth patterns, or turbulent, appearing chaotic and unpredictable. Understanding the physics of laminar-turbulent flow transition has been originally motivated by aerodynamic applications, but has become more widespread since. Initially, hydrodynamic stability was studied by means of the classical linear stability theory investigating the behaviour of small disturbances in space and time around some basic flow state. The exponen-

A. Peplinski · P. Schlatter · D. S. Henningson
Linné FLOW Centre and Swedish e-Science Research Centre (SeRC), KTH Mechanics, Royal Institute of Technology, SE-100 44 Stockholm, Sweden e-mail: adam@mech.kth.se · pschlatt@mech.kth.se · henning@mech.kth.se

P. F. Fischer
MCS, Argonne National Laboratory, 9700 S. Cass Avenue, Argonne, IL 60439, USA e-mail: fischer@mcs.anl.gov

tial growth of linear perturbations is studied at each streamwise position and the distinction between local convective and absolute stability is made [12]. This local treatment is legitimate for parallel and weakly non-parallel flows, but many of the flow configurations developing strong instabilities and eventually exhibiting transition to turbulence are strongly non-parallel and may belong to the open flow category, where fluid particles continuously enter and leave the considered domain. Such unstable open flows require global analysis where the evolution of perturbations is considered in the whole physical domain [6]. The global behaviour of the flow depends on the competition between local instability and basic advection. The extensive work on global stability in the past years has been reviewed *e.g.* in [17].

However, such linear modal analysis often fails in predicting the transitional Reynolds number determined experimentally, and the more accurate transition scenario based on receptivity has to be considered. In this case the non-normality of the linearised Navier-Stokes (LNS) operator has to be taken into account [6, 18] and the global modes of the adjoint operator have to be calculated. This kind of analysis has been performed for the 2D cases *e.g.* the flow past a circular cylinder [9]. The limitations of structural sensitivity analysis are discussed by Chomaz [6], where it was pointed out that this method is better suited for strongly non–parallel flows than for almost parallel flows, as the very high degree of the operator non–normality can lead to wrong predictions of the dynamics.

Although global analysis allows to avoid the limitation of local theory, it is computationally much more expensive, as linear global modes have been associated to the eigenmodes of the LNS operator [10] involving large eigenvalue problems. For sizes of order $\dim(\mathbf{A}) \sim 10^7$ special matrix-free methods using time-steppers are required [2, 3]. Recent advances in numerical methods, in particular tools for solving very large eigenvalue problems [15], make it possible to use linear stability theory for global analysis of 2D and 3D flows with nearly arbitrary complexity, based on only minimal modifications of existing numerical simulation codes [4]. A number of authors have determined the spectrum of the LNS operator for different 2D flows, however, the first calculations for the fully 3D base flow were done by Bagheri *et al*. [3, 16] for a jet in crossflow (JCF). This work has been later extended in [13] by calculating 3D adjoint global eigenmodes.

The objective of the present paper is to demonstrate the use of global linear stability tools developed for the spectral-element code `Nek5000` [8, 7] to investigate the dynamics of flows in moderately complex geometry. As the final case we consider the so-called jet in crossflow which refers to a jet of fluid exiting through a nozzle and interacts with the surrounding cross-flow fluid. It is a canonical flow with complex, fully 3D dynamics which allows for a test of the simulation capabilities and the methods for studying the flow stability. The previous results for this flow [3, 13, 16] were obtained for simplified setups, in which the inflow jet was represented by a Dirichlet boundary condition due to the limitations of the applied pseudo-spectral simulation method. We avoid this limitation using the more flexible spectral-element method (SEM), which provides spectral accuracy while allowing for complex geometries.

2 Direct and adjoint global modes

Structural sensitivity analysis determines the instability mechanism that initiates the transition to an unsteady flow. It combines global linear stability with receptivity looking into the eigenmodes of the LNS (direct) operator $\mathbf{A}$ and its adjoint $\mathbf{A}^\dagger$, where the adjoint operator is defined by the property $\langle \mathbf{u}^\dagger, \mathbf{A}\mathbf{u}\rangle = \langle \mathbf{A}^\dagger\mathbf{u}^\dagger, \mathbf{u}\rangle$, with $\mathbf{u}^\dagger, \mathbf{u}$ and $\langle\cdot,\cdot\rangle$ being vector functions and inner product, respectively. The linear stability analysis of the direct problem let us determine several characteristics: the parameters (*e.g.* Reynolds number) at which the flow first becomes unstable, and the frequencies ω_r, growth rate ω_i and spatial structure of the linear perturbations. On the other hand, the adjoint system provides information on the optimal way to excite the instability, as the perturbation in receptive region amplify more due to forcing. In combination the two types of modes can be used to locate the most sensitive region in the flow known as *wavemaker*, which is defined as the overlap η of the direct $\hat{\mathbf{u}}$ and adjoint $\hat{\mathbf{u}}^\dagger$ strongest global modes [6, 9, 11] (see Figs. 2 and 6),

$$\eta(\mathbf{x}_0) = \frac{|\hat{\mathbf{u}}^\dagger(\mathbf{x}_0)| \cdot |\hat{\mathbf{u}}(\mathbf{x}_0)|}{\langle \hat{\mathbf{u}}^\dagger, \hat{\mathbf{u}}\rangle} \,. \tag{1}$$

The wavemaker is the region in the flow where a variation in the flow structure provides the largest drift of the eigenvalues and therefore pinpoints the most likely region in the flow for the inception of the global instability.

We consider the incompressible Navier–Stokes equations linearised about a base flow $\mathbf{U}_b$ in non-dimensional form with $\mathbf{u}$, p and Re being velocity and pressure perturbation and the Reynolds number, respectively,

$$\frac{\partial \mathbf{u}}{\partial t} + \mathbf{u}\cdot\nabla\mathbf{U}_b + \mathbf{U}_b\cdot\nabla\mathbf{u} - \frac{1}{Re}\nabla^2\mathbf{u} + \nabla p = \mathbf{f}\,, \tag{2}$$

$$\nabla\cdot\mathbf{u} = 0 \quad \text{in } \Omega\,, \tag{3}$$

$$\mathbf{u} = 0 \quad \text{on } \partial\Omega_v\,, \tag{4}$$

$$p\mathbf{n} - \frac{1}{Re}\nabla\mathbf{u}\cdot\mathbf{n} = 0 \quad \text{on } \partial\Omega_o\,. \tag{5}$$

Two last equations are the boundary conditions (BC) on the surface of the computational domain Ω. Subscripts v and o stand for regions where either *velocity* (Dirichlet) or *outflow* BC are specified, and $\mathbf{n}$ denotes the outward normal. The forcing $\mathbf{f}$ usually vanishes inside Ω, but may be used as sponge layers at inflow/outflow boundary. The corresponding set of adjoint equations reads

$$\frac{\partial \mathbf{u}^\dagger}{\partial t} + (\nabla\mathbf{U}_b)^T\mathbf{u}^\dagger - \mathbf{U}_b\cdot\nabla\mathbf{u}^\dagger + \frac{1}{Re}\nabla^2\mathbf{u}^\dagger + \nabla p^\dagger = \mathbf{f}\,, \tag{6}$$

$$\nabla\cdot\mathbf{u}^\dagger = 0 \quad \text{in } \Omega\,, \tag{7}$$

$$\mathbf{u}^\dagger = 0 \quad \text{on } \partial\Omega_v\,, \tag{8}$$

$$p^\dagger\mathbf{n} + \frac{1}{Re}\nabla\mathbf{u}^\dagger\cdot\mathbf{n} = (\mathbf{U}_b\cdot\mathbf{n})\mathbf{u}^\dagger \quad \text{on } \partial\Omega_o\,, \tag{9}$$

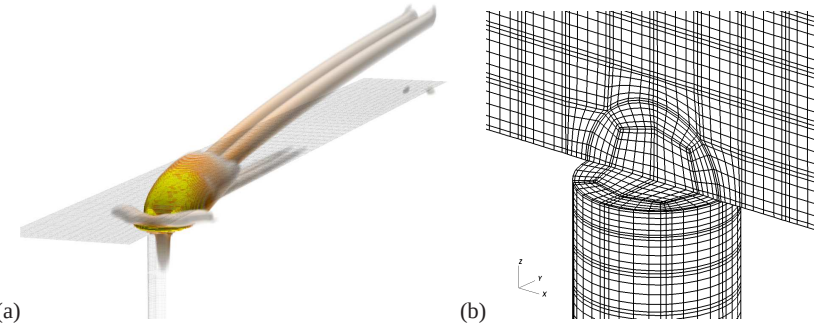

(a) (b)

Fig. 1 (a) Vortical structures (λ_2 isolevels) of the base flow for JCF setup including the pipe. (b) Mesh structure at the connection of the circular pipe with the rectangular box. The element boundary and the position of the GLL points are shown.

where $\mathbf{u}^\dagger$ and $p^\dagger$ are adjoint perturbations. Notice the change of sign in the equations and the fact that *outflow* BC are inhomogeneous.

The solution to the direct and adjoint problem is computed using a Legendre polynomial based SEM implemented in `Nek5000` [8]. In this method the governing equations are cast into weak form and discretised in space by the Galerkin approximation, following the $P_N - P_{N-2}$ approach. The velocity space is spanned by Nth-order Lagrange polynomial interpolants, based on tensor-product arrays of Gauss–Lobatto–Legendre (GLL) quadrature points in a local element. The individual elements take the shape of hexahedra which can then be transformed using general coordinate mapping as shown in Fig. 1(b).

`Nek5000` does not support the general inhomogeneous BC as given above. Therefore, to keep direct and adjoint problems consistent we set homogeneous Dirichlet BC on all $\partial\Omega$. To avoid reflections we use a sponge forcing $\mathbf{f} = \lambda(\mathbf{x})(\mathbf{U}_b - \mathbf{v})$ at the inflow/outflow boundaries, where $\mathbf{v}$ stands for $\mathbf{u}$ or $\mathbf{u}^\dagger$ and $\lambda(\mathbf{x})$ is a smooth step function [5]. The dependency of the operator spectra on the applied BC for the flow past circular cylinder case is discussed in Section 4.

To obtain the base flow one has to find the steady state solution of the nonlinear Navier–Stokes equations, which in many of the considered cases is unstable, in particular for strongly convectively unstable flows (*e.g.* JCF). We compute the base flow using selective frequency damping (SFD) [1], which damps the oscillations of the unsteady part of the solution using a temporal low-pass filter by setting $\mathbf{f} = -\chi(\mathbf{u} - \mathbf{w})$, where $\mathbf{u}$ is the flow solution and $\mathbf{w}$ its temporally low-pass-filtered counterpart obtained by a differential exponential filter $\mathbf{w}_t = (\mathbf{u} - \mathbf{w})/\Delta$. The amplitude of the forcing $\varepsilon = \|(\mathbf{u} - \mathbf{w})\|$ in Ω is a good indicator of convergence; 2D test cases reached levels $\varepsilon \approx 10^{-13}$, whereas the computationally more expensive 3D runs were stopped at 10^{-10} or 10^{-7} depending on the resolution, which is lower than the tolerance used for eigenvalue calculation (10^{-6}). An example of such a SFD base flows for JCF and cylinder flow are presented in Figs. 1(a) and 2.

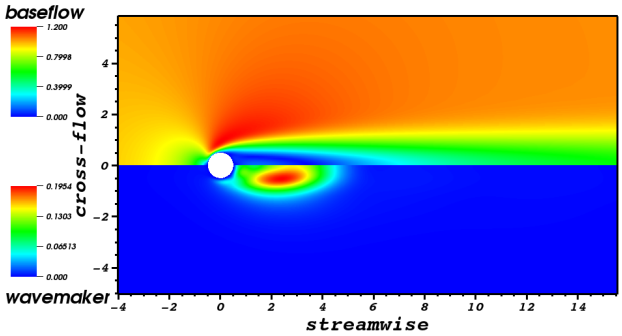

Fig. 2 Two-dimensional flow past a circular cylinder at $Re = 50$. The upper part shows the velocity magnitude of the base flow, and the lower part presents the overlap function η for the strongest direct and adjoint modes. This plot can be compared with Figs. 8 and 17 in Ref. [9].

The eigenvalue problem is then constructed rewriting the LNS equations in operator form $\mathbf{u}_t = \mathbf{A}\mathbf{u}$ and assuming $\mathbf{u}(\mathbf{x},t) = \hat{\mathbf{u}}(\mathbf{x})\exp(-i\omega t)$, where $\hat{\mathbf{u}}(\mathbf{x})$ is the global mode and ω its complex eigenvalue. For general 3D flows the size of the matrix $\mathbf{A}$ prohibits its explicit construction, so only the action of $\mathbf{A}$ on the vector $\mathbf{u}$ can be calculated. Solving the eigenvalue problem can then be achieved using the so-called time-stepper method, *i.e.* an iterative technique based on orthogonal projection of $\mathbf{A}$ onto a lower-dimensional subspace, in which the Arnoldi algorithm is applied and the Krylov subspace is constructed using snapshots taken from the evolution of the flow field $\mathbf{u}$ separated by a constant time interval Δt. To avoid frequency aliasing Δt must be small enough such that at least two sampling points in one period of the highest frequency mode are included (see *e.g.* Ref. [2]). In presented studies we do not consider dependency of calculated spectra on the size of Krylov space and Δt. The other important parameter is the actual time step δt of the simulation, which is related to the CFL condition. In our simulations we have tested Courant numbers in the range $0.05 - 0.2$ and found significant dependency of the operator $\mathbf{A}$ spectra if the cases were marginally resolved in space. On the other hand, the fully resolved 2D simulations show little dependence of the spectra on the Courant number.

In our implementation we use the implicitly restarted Arnoldi method (IRAM) from the ARPACK library [15]. We solve for the generalised eigenvalue problem $\mathbf{A}\hat{\mathbf{u}} = -i\omega\mathbf{B}\hat{\mathbf{u}}$, where $\mathbf{B}$ is the mass matrix. It allows us to simplify the treatment of the duplicated values of the velocity field at the element faces, and to get the exact value of the inner product applied in the orthogonalisation step.

3 Poiseuille Flow

To validate our implementation we performed a number of tests corresponding to different flow configurations. The first one is plane Poiseuille flow, in which a fluid is moving laterally between two plates whose length and width is much greater

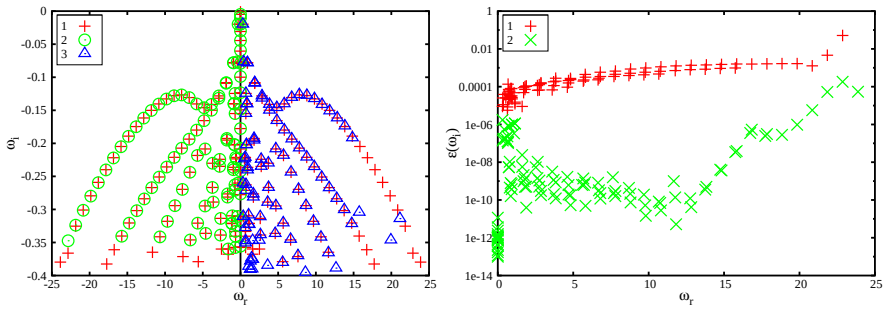

Fig. 3 Spectra (growth rate ω_i versus frequency ω_r) for the different simulations of plane Poiseuille flow at $Re = 2000$. We utilise the negative and positive ω_r parts to compare different cases. Left: Comparison of the spectra of `Nek5000` run with $N = 17$ (1) with results of the local analysis (2) and the low resolution $N = 11$ (3). Right: Relative error of the growth rate $\varepsilon(\omega_i)$ for $N = 17$ as a function of ω_r with respect to local analysis (1) and the spectra of the adjoint operator (2).

than the distance separating them. This 2D parallel flow can be treated exactly by local analysis. We performed our calculations for $Re = 2000$ (based on centreline velocity and channel half height) on a rectangular grid of streamwise length 2π with periodic BC, built of 6×6 spectral elements with polynomial order N ranging from 11 to 17. We compared our result with local analysis (O. Tammisola, private communication) and found very good match for the first 100 eigenvalues calculated for $N = 17$ (Fig. 3). Although only 3 modes with the highest frequency $\omega_r > \omega_{max} \approx 21$ are visibly displaced, we can see slow decrease of accuracy with growing ω_r. This becomes more pronounced with decreasing N as the maximum frequency of the well resolved waves ($\omega_{max} \approx 16$ for $N = 11$) is getting lower and thus a small number of spurious modes appears. Similar conclusions can be drawn comparing direct and adjoint modes, however the threshold frequency for fast relative error growth appears to be lower ($\omega_{max} \approx 12$ for $N = 17$). There is also a number of modes clustered around $\omega_r = 0$, with relative error of order 10^{-6} which all correspond to highly damped modes.

4 Flow Past Circular Cylinder

The next case is the plane wake behind a circular cylinder, which is a canonical 2D, non-parallel flow extensively studied in the literature. Its structural sensitivity was investigated in Ref. [9] and we compare our results against this work adopting the grid from [14], where the cylinder of unit diameter was placed at (0,0) in the grid extending from -15 to 35 and from -15 to 15 in streamwise and cross-flow directions, respectively. We performed a number of runs for $Re = 40$, 45 and 50 (based on diameter and incoming velocity) calculating the most unstable global modes and their overlap function η. Very good agreement with [9] is obtained. An example of a base flow and a wavemaker for $Re = 50$ is presented in Fig. 2 which can readily

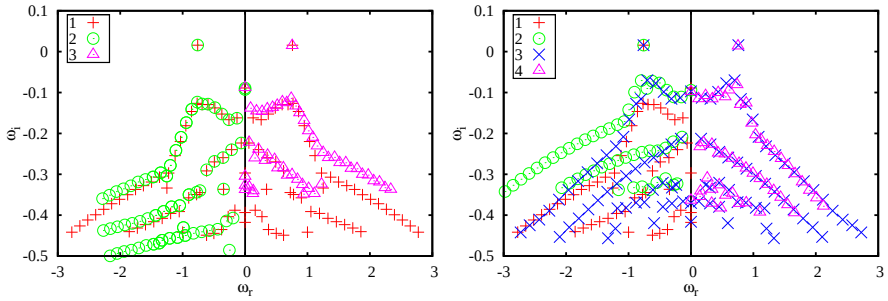

Fig. 4 Spectra of the direct operator for the flow past circular cylinder at $Re = 50$. Left: Case with outflow BC in the non-symmetric box (1) compared with results of the CPL code (2) and run in the symmetric box (3). Right: Cases in non-symmetric box with different BC: (1) outflow (the same as (1) on left plot), (2) Dirichlet without sponge, (3) Dirichlet with sponge applied to inflow/outflow regions. (4) symmetric box with Dirichlet BC and sponge.

be compared with Figs. 8 and 17 in Ref. [9]. The left plot in Fig. 4 (negative ω_r) presents the comparison of the calculated spectra of the direct operator for $Re = 50$ with the results of CPL code, which is a modified version of the code employed in [9] (I. Lashgari, private communication). There is good agreement for the least damped, low frequency modes, but we observe a relative shift of the modes growths with increasing ω_r and decreasing ω_i. These weaker modes are very sensitive to the exact simulations details such as grid size and boundary conditions. Furthermore, we present results of the runs with outflow BC (Eq. 5) for non-symmetric ($x \in [-15, 35]$; crosses) and symmetric ($x \in [-35, 35]$; triangles) mesh; the two meshes differ in the extent of the upstream (inflow) part which is important for the adjoint simulations. There is clearly sensitivity of the spectra to these details as the position of the branches is moved. The dependency of the spectra on the applied BC and grid size is illustrated in Fig. 4. We found the Dirichlet BC combined with the sponge forcing $\mathbf{u}$ and $\mathbf{u}^\dagger$ at inflow/outflow to be the least sensitive to the grid and we thus use these settings in the remainder of our study. The relative error of the growth rate pertaining to the direct and adjoint modes for this setup is lower than 10^{-6} (not shown). The resolution studies for this case showed strong dependency of the spectra on the polynomial order N with the frequency of the poorly resolved modes shifted towards $\omega_r = 0$.

5 Jet in Crossflow

The most complex flow case considered in this study is the jet in crossflow (JCF), which is a non-parallel and fully 3D flow referring to a jet of fluid exiting a pipe and interacting with the boundary layer perpendicular to the pipe orifice (see Fig. 1). For the detailed description of the case we refer to Refs. [3, 13]. We consider two different setups of this flow: one corresponding the simplified setup of Ilak *et al.* [13],

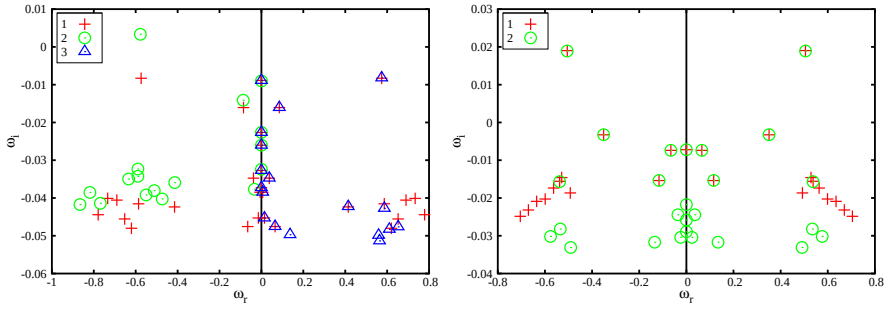

Fig. 5 The spectra of the direct and adjoint operator for JCF for velocity ratio $R = 1.5$. Left plot corresponds to the simplified setup discarding the pipe and presents the direct operator spectra for high (1) and low (2) resolution runs together with the adjoint operator spectra of the high resolution run (3). The right plot shows the spectra of the direct (1) and adjoint (2) operator for the setup including pipe in the consideration.

in which the inflow jet was represented by a Dirichlet boundary condition, and the more realistic one with the pipe included in the domain as shown in Fig. 1. For the simplified setup, we made two major changes compared to Ref. [13]: i) no fringe region as the SEM code does not require periodic BC in the streamwise direction, and ii) the length of the box is longer (150 versus 75 units in [13]). We increased the box length because we found the result to be very sensitive to any kind of disturbances; especially the proper treatment of outflow BC proved to be crucial, so in an effort to reduce its influence we increased the downstream part of the grid together with a sponge region. This extreme sensitivity of the simplified JCF can be related to both strong non-normality of LNS operator, but also to the "unphysical" $\mathbf{u} = 0$ Dirichlet BC at the pipe orifice, which is very close to the dynamically important region. For the same reason we were not able to reproduce the results of [13]. In our runs we set the jet to free-stream velocity ratio R to 1.5, and the Reynolds number at the jet position $Re = 178.2$ (based on free-stream velocity and cross-flow displacement thickness). The jet diameter and pipe length are equal 3 and 20 units, respectively.

Most of our runs we performed studying the simplified setup and we found it very sensitive to the grid resolution. On the left plot in Fig. 5 the results of the higher resolution (polynomial order $N = 9$, crosses) are compared with the lower resolution ($N = 6$, circles) and the spectra of the adjoint operator ($N = 9$, triangles). The increased resolution causes the initially unstable flow (positive growth rate of the strongest mode) to stabilise, as the whole spectra shifts down. Comparison of the direct and adjoint spectra also shows that the even $N = 9$ resolution is only marginal, as the lowest value of the growth rate error $\varepsilon(\omega_i)$ is on the order of 10^{-4}.

Similar conclusions can be drawn comparing the direct (crosses) and adjoint (circles) spectra of the high resolution ($N = 9$) run including the pipe (right plot in Fig. 5). One can see a clustering of the poorly resolved adjoint modes around $\omega_r = 0$, which is similar to what we already observed in the cylinder case (Section 4). However, the least stable modes agree well between direct and adjoint simulation indicating that the main dynamics is captured well. Fig. 6 presents a 2D cut through

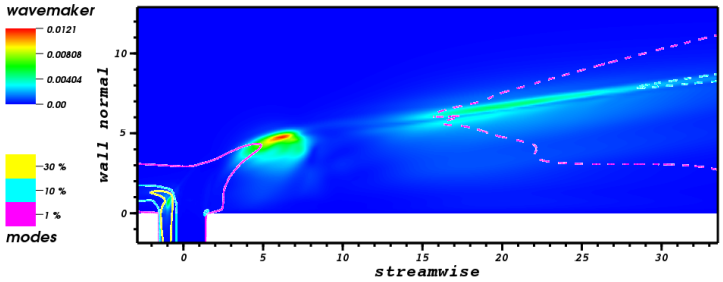

Fig. 6 Two-dimensional cut through the symmetry plane of the grid for the JCF setup including the pipe for $R = 1$. The colours shows the value of the strongest overlap η. Isolevels of the direct (dashed line) and adjoint (continuous line) strongest modes at 1%, 10% and 30% are also shown.

the symmetry plane of the grid showing isosurfaces of the direct (dashed) and adjoint (continuous line) strongest modes as well as their overlap η (colour). The isocontours are placed at 1%, 10% and 30% of the maximum value of the modes showing their spatial extent and illustrating considerable separation of their maxima, which is related to the strong non-normality of the operator. As the plot covers the region close to the pipe orifice, only the adjoint mode maximum is visible. The overlap function η features a total of three maxima of which one is clearly related to the adjoint mode, located close to the steady horseshoe vortex upstream the jet. The other two maxima appear in the shear layer downstream of the jet forming the wavemaker.

The analysis of 3D flows is computationally very expensive, and the computation of the single JCF spectrum with $N = 9$ takes about 2–3 weeks on 1024 cores.

6 Conclusions

In this work we investigated the use of linear stability tools implemented in the SEM code `Nek5000` for studying the stability and sensitivity of 3D flows with moderately complex geometry. We validated our implementation on a number of 2D parallel and non-parallel flow cases against the local stability analysis as well as literature data. Resolution studies show that the calculated spectra are very sensitive to the grid resolution and proper treatment of boundary conditions. In our simulations we adopted Dirichlet boundary conditions together with sponge layers to keep direct and adjoint problems consistent, however another possible solution would be to adopt correct direct and adjoint outflow boundary according to Eqs 5 and 9. The grid spacing defines the shortest wave length that can be properly resolved, which corresponds to setting the maximum possible frequency of the calculated modes. Higher modes then appear as spurious modes in the spectrum. In the case of the flow past cylinder and a jet in crossflow (including the inflow pipe) the frequency of the spurious modes was shifted towards zero giving clusters of spurious low fre-

quency modes with low growth rates. Comparing direct and adjoint spectra is shown to help in identifying spurious modes, but even then careful resolution studies are necessary. The dependency of the spectra on the grid resolution usually does not play a crucial role for 2D simulations, but it becomes an important issue when moving to 3D, in particular in regions of active dynamics and complex geometry. In this case adaptive mesh refinement algorithms might be instrumental for future studies.

Acknowledgements We would like to thank O. Tammisola and I. Lashgari for help in developing and testing our implementation. Computer time was provided by Swedish National Infrastructure for Computing (SNIC). The third author was supported by the U.S. Department of Energy under Contract DE-AC02-06CH11357.

References

1. Åkervik, E., Brandt, L., Henningson, D.S., Hœpffner, J., Marxen, O., Schlatter, P.: Steady solutions of the Navier-Stokes equations by selective frequency damping. Phys. Fluids **18**(068102), 1–4 (2006)
2. Bagheri, S., Åkervik, E., Brandt, L., Henningson, D.S.: Matrix-free methods for the stability and control of boundary layers. AIAA J. **47**, 1057–1068 (2009)
3. Bagheri, S., Schlatter, P., Schmid, P.J., Henningson, D.S.: Global stability of a jet in crossflow. J. Fluid Mech. **624**, 33–43 (2009)
4. Barkley, D., Gomes, M.G.M., Henderson, R.D.: Three-dimensional instability in flow over a backward-facing step. J. Fluid Mech. **473**, 167–190 (2002)
5. Chevalier, M., Schlatter, P., Lundbladh, A., Henningson, D.S.: SIMSON: a pseudo-spectral solver for incompressible boundary layer flows. Tech. Rep. 2007:07, KTH Mechanics (2007)
6. Chomaz, J.M.: Global Instabilities in Spatially Developing Flows: Non-Normality and Nonlinearity. Annu. Rev. Fluid Mech. **37**, 357–392 (2005)
7. Fischer, P., Lottes, J., Kerkemeier, S.: nek5000 Web page (2008). http://nek5000.mcs.anl.gov
8. Fischer, P.F.: An Overlapping Schwarz Method for Spectral Element Solution of the Incompressible Navier Stokes Equations. J. Comput. Phys. **133**, 84–101 (1997)
9. Giannetti, F., Luchini, P.: Structural sensitivity of the first instability of the cylinder wake. J. Fluid Mech. **581**, 167–197 (2007)
10. Henningson, D.S., Åkervik, E.: The use of global modes to understand transition and perform flow control. Phys. Fluids **20**(3), 031,302 (2008)
11. Hill, D.C.: Adjoint systems and their role in the receptivity problem for boundary layers. J. Fluid Mech. **292**, 183–204 (1995)
12. Huerre, P., Monkewitz, P.A.: Local and global instabilities in spatially developing flows. Annu. Rev. Fluid Mech. **22**, 473–537 (1990)
13. Ilak, M., Schlatter, P., Bagheri, S., Henningson, D.S.: Bifurcation and stability analysis of a jet in cross-flow: onset of global instability at a low velocity ratio. J. Fluid Mech. **696**, 94–121 (2012)
14. Lashgari, I., Pralits, J.O., Giannetti, F., Brandt, L.: First instability of the flow of shear-thinning and shear-thickening fluids past a circular cylinder. J. Fluid Mech. **701**, 201–227 (2012)
15. Lehoucq, R.B., Sorensen, D.C., Yang, C.: ARPACK users guide: Solution of large scale eigenvalue problems by implicitly restarted Arnoldi methods. (1997)
16. Schlatter, P., Bagheri, S., Henningson, D.S.: Self-sustained global oscillations in a jet in crossflow. Theor. Comput. Fluid Dyn. **25**, 129–146 (2011)
17. Theofilis, V.: Global Linear Instability. Annu. Rev. Fluid Mech. **43**, 319–352 (2011)
18. Trefethen, L.N., Trefethen, A.E., Reddy, S.C., Driscoll, T.A.: Hydrodynamic stability without eigenvalues. Science **261**, 578–584 (1993)